Hindawi
Advances in Civil Engineering
Volume 2023, Article ID 5668254, 18 pages
https://doi.org/10.1155/2023/5668254

Research Article

Deformation Analysis of a New Subway Transfer Channel Closely Undercrossing an Existing Station

Houqiang Sun,[1] Jun Wu,[1] Jiabing Zhang,[2] Yu Du,[1] Lirong Teng,[1] and Houtong Qin[2]

[1]*CCTEB Infrastructure Construction Investment Co. Ltd., Wuhan, Hubei 430073, China*
[2]*College of Civil Engineering and Architecture, Guangxi University, Nanning 530004, China*

Correspondence should be addressed to Jiabing Zhang; zhang.j.b@gxu.edu.cn

Received 30 May 2023; Revised 5 August 2023; Accepted 9 August 2023; Published 30 September 2023

Academic Editor: Jorge Branco

Copyright © 2023 Houqiang Sun et al. This is an open access article distributed under the Creative Commons Attribution License, which permits unrestricted use, distribution, and reproduction in any medium, provided the original work is properly cited.

Disturbances that occur due to the construction of new subway transfer channels in cities pose a significant threat to the safe operation and structural stability of existing subway stations. Due to the construction of the new Jin-Fu Station of Chengdu Rail Transit Line 27, the transfer channel of the new Jin-Fu Station closely underpasses the station of the existing Metro Line 6. First, based on the random medium theory, the curved integral boundaries of the rectangular section are improved and simplified by the numerical simulation. Second, the mechanical response of the underpass construction to the existing subway station is analyzed by Pasternak foundation model theory. Finally, the accuracy of the theoretical calculation is verified by the three-dimensional numerical calculation and the measured data, and the sensitivity of its parameters is analyzed. The results show that maintaining a certain net distance d (that is, increasing the thickness of the interlayer soil) is conducive to forming the soil arch effect and reducing the deformation of the existing station above. The settlement of the existing station can be reduced by increasing the height-to-width ratio of the excavated section, but the maximum bending moment of the floor will increase slightly. With the increase in the foundation reaction coefficient k, the interaction between the soil mass and the existing station is enhanced, and the deformation, bending moment, and shear force on the floor of the existing station increase significantly. When the foundation reaction coefficient increases to $10k$, there is an obvious uplift phenomenon outside the settlement trough of the existing station floor.

1. Introduction

With the rapid development of urban rail transit in China, subway station projects are increasingly being developed in deeper and more complex underground environments. New projects will inevitably cross existing underground structures in various forms, including lateral crossings, multiangle crossings, close-range crossings, ultralow clearance crossings, and closely spaced crossings [1–4]. Compared with the construction of other forms, the construction of a closely spaced underpass segment is more likely to cause settlement, inclination, and even overturning of the existing structures [5], posing significant safety risks. Therefore, how to ensure the stability and safety of the existing structures during the construction of a new subway station's closely spaced underpass must urgently be determined for the rail transit construction.

Currently, many scholars have conducted valuable research on the impact of new tunneling construction on existing underground structures through theoretical calculations, numerical simulations, and field measurements. In terms of theoretical research, existing studies have mainly established relevant prediction models based on the different calculation theories depending on the specific engineering conditions. For example, regarding the undercrossing of existing tunnels by new tunnels, Zhou et al. [6] proposed a prediction model for the deformation of existing tunnel structures caused by undercrossing construction based on the layer-by-layer method. They found that the deformation of existing underground structures induced by undercrossing construction is not only influenced by the soil excavation unloading and the stiffness of the structures themselves but also closely related to the factors such as the shape of the excavation section and the area of excavation. Liu et al. [7] proposed a superposition method based on the elastic foundation beam theory to calculate the changes in the mechanical properties of existing tunnels caused by the excavation of

the new tunnel below, and the accuracy of the theoretical calculation results was successfully verified through numerical simulations. For the undercrossing of new tunnels and existing pipelines, underground corridors, and other structures, Zhao et al. [8] established a mechanical model and analysis method for the double-layer presupport system (DLPS) of large-scale existing underground corridor projects crossing through water-rich sand layers based on the elastic foundation beam theory. The calculated settlement results were compared with the measured settlement results for verification, and the established model can reflect the interaction characteristics among the upper presupport, lower presupport, and middle soil. Liu et al. [9] proposed an analytical solution to predict the deformation and settlement trends of existing pipelines caused by shield tunneling undercrossing. By analyzing the spatial and temporal characteristics of the deformation of the existing pipeline and combining the deformation of known points on the pipeline, the entire pipeline's spatial and temporal deformation can be inferred. Wei et al. [10] studied the deformation problem of new shield tunnels undercrossing existing tunnels using the shear dislocation model. The results showed that the settlement of existing tunnels is not only affected by the size and shape of the excavation section but also disturbed by the additional thrust of the cutterhead, the frictional force of the shield shell, and the additional pressure of grouting during the undercrossing of the new tunnel, leading to excessive deformation of the existing tunnels.

In addition, to more intuitively demonstrate and analyze the disturbance of existing structures caused by new tunnel undercrossing, existing studies often use three-dimensional numerical calculations. For example, Wang et al. [11] established a three-dimensional model of the undercrossing of existing pipelines by a proposed station using FLAC3D finite difference software to study the influence of different factors during the construction phase of the pile and shell station on the surface and pipeline settlement and analyze the deformation of adjacent underground pipelines caused by the construction of the new tunnel. The results showed that the maximum settlement of the pipeline increases with the increasing pipeline burial depth. Ke et al. [12] studied the undercrossing of existing pipelines by new tunnels and concluded that the larger the excavation area of the new tunnel is, the greater the vertical displacement and bending moment of the existing pipeline. Lai [13], based on monitoring data and finite difference method (FDM) numerical simulations, analyzed the settlement characteristics of the undercrossing of existing tunnels at small angles and close distances and found that as the new undercrossing tunnel advances, the settlement trough of the existing tunnel becomes wider and deeper.

The above studies mainly focus on the case of new subway tunnels undercrossing existing tunnels, pipelines, and other structures, with few studies addressing the situation where new large-section rectangular stations undercross the existing stations. The disturbances caused by the undercrossing construction of new large-section rectangular stations are much greater than those caused by the undercrossing construction of new subway tunnels at close distances/ultrasmall clearances. As the layout of subway lines becomes more complex, it becomes increasingly important to understand the deformation and disturbance caused by the undercrossing of new subway stations to existing stations. Based on this, this paper relies on the construction practice of the undercrossing of the new transfer passage of Jin-Fu Station on Chengdu Rail Transit Line 27 to the existing Metro Line 6 station. The theoretical calculation of the deformation induced by the undercrossing construction is carried out using the two-stage method, and then the deformation characteristics of the existing station structure are analyzed using a three-dimensional numerical calculation method to verify the rationality of the theoretical calculation and reveal the deformation characteristics of the new subway transfer passage undercrossing the existing station to provide a reference for similar undercrossing construction.

2. Calculation of the Mechanical Response of the Existing Station Induced by Undercrossing Construction Based on the Two-Stage Method

This section mainly adopts the two-stage method to analytically calculate the settlement of the existing station structure. In the first stage, the random medium theory is improved, and after obtaining the settlement curve of the soil layers, it is converted into a displacement load applied to the existing station structure. In the second stage, based on the calculation model of the first stage, the Pasternak foundation model is used for theoretical calculation to obtain the settlement of the existing station.

2.1. Calculation of the Settlement of the Existing Station's Roof Soil Layer. Random media theory was proposed by Polish scholar Litwiniszyn [14]. With random media theory, the excavation of a tunnel section can be treated as a plane strain problem and, combined with probability theory and statistics, the tunnel excavation can be decomposed into an infinite number of small blocks. The ground deformation caused by tunnel excavation is then equivalent to the sum of the deformations caused by an infinite number of small block excavations. As shown in Figure 1, an infinitely small unit has a length, width, and height defined as $d\xi$, $d\zeta$, and $d\eta$, respectively, and the subsidence caused by the excavation of the unit is denoted as $W_e(X, Y, Z)$.

For the sake of convenience in the study, it is assumed that the soil consolidation is undrained and that the volume of the final settlement of the ground surface is equal to the volume of the stratum excavation loss. Therefore, when the unit body completely sinks, its volume can be expressed as $d\xi d\zeta d\eta$. Taking the center of the excavation unit as the coordinate origin, the settlement of any point (X, Y, Z) in the stratum can be obtained as follows:

$$W_e(X, Y, Z) = \frac{1}{r(Z)} \exp\left[-\frac{\pi \tan^2 \beta}{r^2(Z)} (X^2 + Y^2)^2\right] d\xi d\zeta d\eta, \tag{1}$$

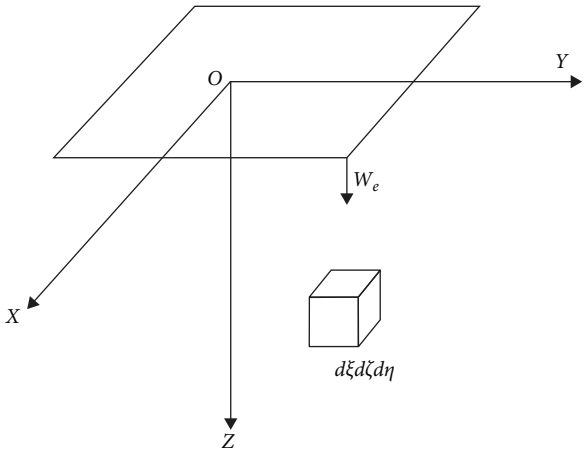

Figure 1: Schematic diagram of the unit excavation.

where $r(Z)$ is the influence radius in the Z direction during excavation, which can be calculated with the stratum influence angle β, and it depends on the on-site monitoring data or geological exploration observations.

The stratum influence angle can be calculated by the following formula [15]:

$$\tan\beta = \frac{20^{\circ}}{50^{\circ} - \phi}. \tag{2}$$

During the excavation of the tunnel, the strain along the central axis of the tunnel is zero, so the process can be regarded as a plane strain problem. Moreover, integrating Equation (1) over an infinite interval in the Y direction yields:

$$\begin{aligned} W_e(X,Z) &= \iint_{\Omega} d\xi d\eta \int_{-\infty}^{+\infty} \frac{\tan\beta}{\eta} \\ &\quad \exp\left\{-\frac{\pi\tan^2\beta}{\eta^2}\left[(X-\xi)^2 + (Y-\zeta)\right]^2\right\} d\zeta \\ &= \iint_{\Omega} \frac{\tan\beta}{\eta} \exp\left[-\frac{\pi\tan^2\beta}{\eta^2}(X-\xi)^2\right] d\xi d\eta. \end{aligned} \tag{3}$$

After excavation, the tunnel will not completely collapse under support but will undergo deformation, with the cross-sectional area A relative to the original size of a; at this time, the ground settlement $W_e(X, Z)$ should be the difference between the two:

$$W_e(x,z) = \iint_{A-a} \frac{\tan\beta}{\eta - z} \exp\left[-\frac{\pi\tan^2\beta}{(\eta - z)^2}(x-\xi)^2\right] d\xi d\eta. \tag{4}$$

Currently, most of the tunnel cross-sections studied using this theory are uniformly or nonuniformly convergent

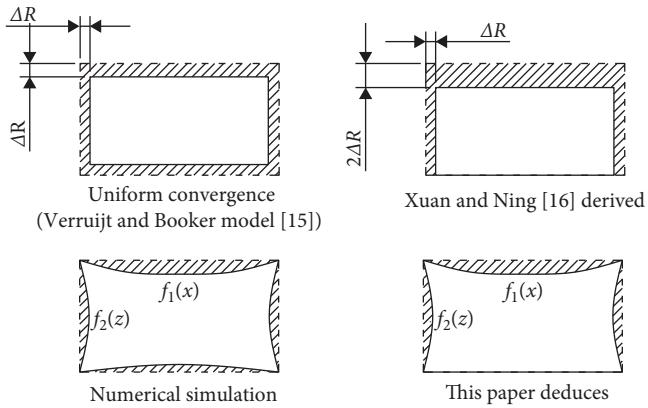

Figure 2: Sectional convergence of the rectangular tunnel.

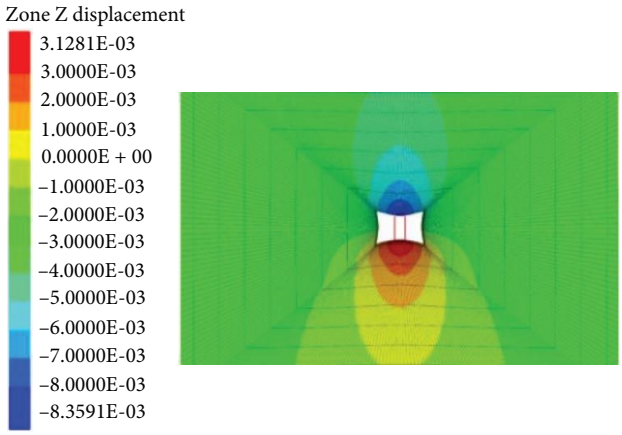

Figure 3: Numerical simulation of the convergence of a rectangular tunnel section.

circular or elliptical cross-sections. There are relatively few analyses of nonuniformly convergent rectangular cross-sections. As shown in Figure 2, Xuan and Ning [16] derived the calculation formula for the nonuniform convergence mode of rectangular tunnel cross-sections, and Verruijt and Booker [17] regarded the convergence of a tunnel as uniform; however, the deformed rectangular cross-section they used still had a straight-sided shape, which deviates from actual situations. In fact, the force situation of the support of a rectangular tunnel is very complex. Under the action of soil pressure, its support deformation is no longer straight and should exhibit a curved shape with a tendency for greater deformation in the middle and smaller deformation on both sides. When a tunnel is excavated, its bottom will always produce a bulging phenomenon, which is caused by stress release rather than ground loss. Therefore, in this paper, it is assumed that the deformation of the tunnel bottom is 0 when calculating ground displacement, and a rectangular cross-section convergence model is established based on this.

To further analyze and verify the deformation characteristics and actual situation of the cross-section of a rectangular tunnel after excavation, numerical simulation analysis is used to verify the convergent deformation of the rectangular section after excavation, as shown in Figure 3. The width and

height of the rectangular tunnel are 23 m and 9 m, respectively, with a burial depth of 25 m. The soil parameters are obtained by the weighted average from the homogeneous soil layer, and the gravity density is 21 kN/m^3. The elastic modulus is 33.7 MPa, the cohesive force c of the sand–gravel layer is 0, the internal friction angle is 35°, and Poisson's ratio is 0.31. The shell element is used to simulate the concrete lining, with a lining thickness of 50 cm and a strength grade of C35 concrete. The supporting pile was simulated using the built-in pile element in FLAC3D, with a diameter of 1.0 m, a Young's modulus of 8×10^4 MPa, a Poisson's ratio of 0.3, a shear coupling spring unit length stiffness of 6×10^{10} N/m, a friction angle of 10° for the normal coupling spring, and a normal coupling spring unit length stiffness of 1.3×10^{11} N/m. The simulation results showed that the deformation of the rectangular section was different than the nonuniform convergence mode analyzed by Xuan and Ning [16], and its section boundary was a curve rather than a straight line. According to the numerical simulation results, the curve section boundary is more reasonable.

Due to the different depths of the tunnels, the pressure of the surrounding rock they are subjected to varies, which results in different degrees of contraction of their cross-sections. Therefore, in this paper, nine rectangular tunnels with different depths were selected to investigate the upper deformation, as shown in Figure 4. Although the maximum vertical displacement of the tunnels with different depths is different, the contour lines of the tunnel cross-section contraction are basically consistent with the conclusion derived in this paper, which verifies that the boundary of the convergence of the rectangular tunnel cross-section is a curve. Based on the above verification and assumptions and the Chengdu Metro Line 27 project, a calculation model for the convergence of rectangular tunnel cross-section is obtained by selecting a tunnel with a burial depth of $H = 25$ m, as shown in Figure 5. Taking the midpoint of the unconverted section of the excavated tunnel as the origin, Gauss fitting of the convergence curve of the cross-section is performed, and the upper limit of the integral of the tunnel cross-section deformation $f_1(x)$ and $f_2(z)$ is obtained.

After obtaining the integral boundaries of the rectangular tunnel, the formula for calculating the settlement of any stratum can be calculated by Equation (4):

$$W_e(x,z) = \int_a^b \int_c^d \frac{\tan\beta}{\eta - z} \exp\left[-\frac{\pi \tan^2\beta}{(\eta - z)^2}(x-\xi)^2\right] d\xi d\eta - \int_e^f \int_g^h \frac{\tan\beta}{\eta - z} \exp\left[-\frac{\pi \tan^2\beta}{(\eta - z)^2}(x-\xi)^2\right] d\xi d\eta, \tag{5}$$

where a, b, c, and d are the integral bounds before the tunnel section converges and e, f, g, and h are the integral bounds after the tunnel section converges.

The boundary curves $f_1(x)$ and $f_2(x)$ are related to the tunnel depth, cross-sectional size, and ground loss. The following equation is obtained through numerical simulation and Gauss fitting:

$$f_1(x) = \frac{-2u_1}{\sqrt{\pi/2}} e^{-8\left(\frac{x}{B}\right)^2}, \tag{6}$$

$$f_2(z) = \frac{-2u_2}{\sqrt{\pi/2}} e^{-8\left(\frac{z}{A} + 0.05\right)^2}, \tag{7}$$

where u_1 and u_2 are the section convergence coefficients, which are related to the section size, burial depth, and formation loss rate. The specific calculation is as follows:

$$u_1 = \frac{V_i AB}{16(A+B)}\left(2 - e^{-\frac{H}{B}}\right), \tag{8}$$

$$u_2 = \frac{(A+B) - \sqrt{(A+B)^2 - 4ABV_i}}{32} K\left(2 - e^{-\frac{H}{A}}\right). \tag{9}$$

In the above formula, A is the height of the excavation surface, B is the width of the excavation surface, H is the burial depth of the central point of the tunnel, K is the lateral pressure coefficient, and V_i is the formation loss rate. Wang et al. [18] provided the influence of different construction methods on the formation loss rate, as shown in Table 1.

Because the integrands in Equation (5) do not have primitive functions, most scholars currently use the Gauss—Legendre integration method in the numerical integration of the calculation. However, due to the complexity of the integration interval, it is not easy to obtain the calculation result. Qiang et al. [19] improved the theory of random media for circular tunnels but did not consider the case of rectangular tunnels. Therefore, in this paper, the solution of the theory of random media is simplified to obtain the following formula:

$$W_e(x,z) = AB\frac{\tan\beta}{H - z} \exp\left[-\frac{\pi \tan^2\beta}{(H-z)^2} x^2\right] - (B - 2u_2)(A - u_1)\frac{\tan\beta}{H - z} \exp\left[-\frac{\pi \tan^2\beta}{(H-z)^2} x^2\right], \tag{10}$$

where A is the height of the excavation face, B is the width of the excavation face, and H is the burial depth of the center point of the tunnel.

Since the convergence value of the tunnel section is relatively small compared to the width and height of the tunnel, the product of the convergence values can be ignored, and the above formula can be simplified to:

$$W_e(x,z) = (Bu_1 + 2Au_2)\frac{\tan\beta}{H - z} \exp\left[-\frac{\pi \tan^2\beta}{(H-z)^2} x^2\right]. \tag{11}$$

2.2. Calculation of the Mechanical Response of the Existing Stations. In this paper, the Pasternak foundation model is used to calculate the settlement of existing structures, with

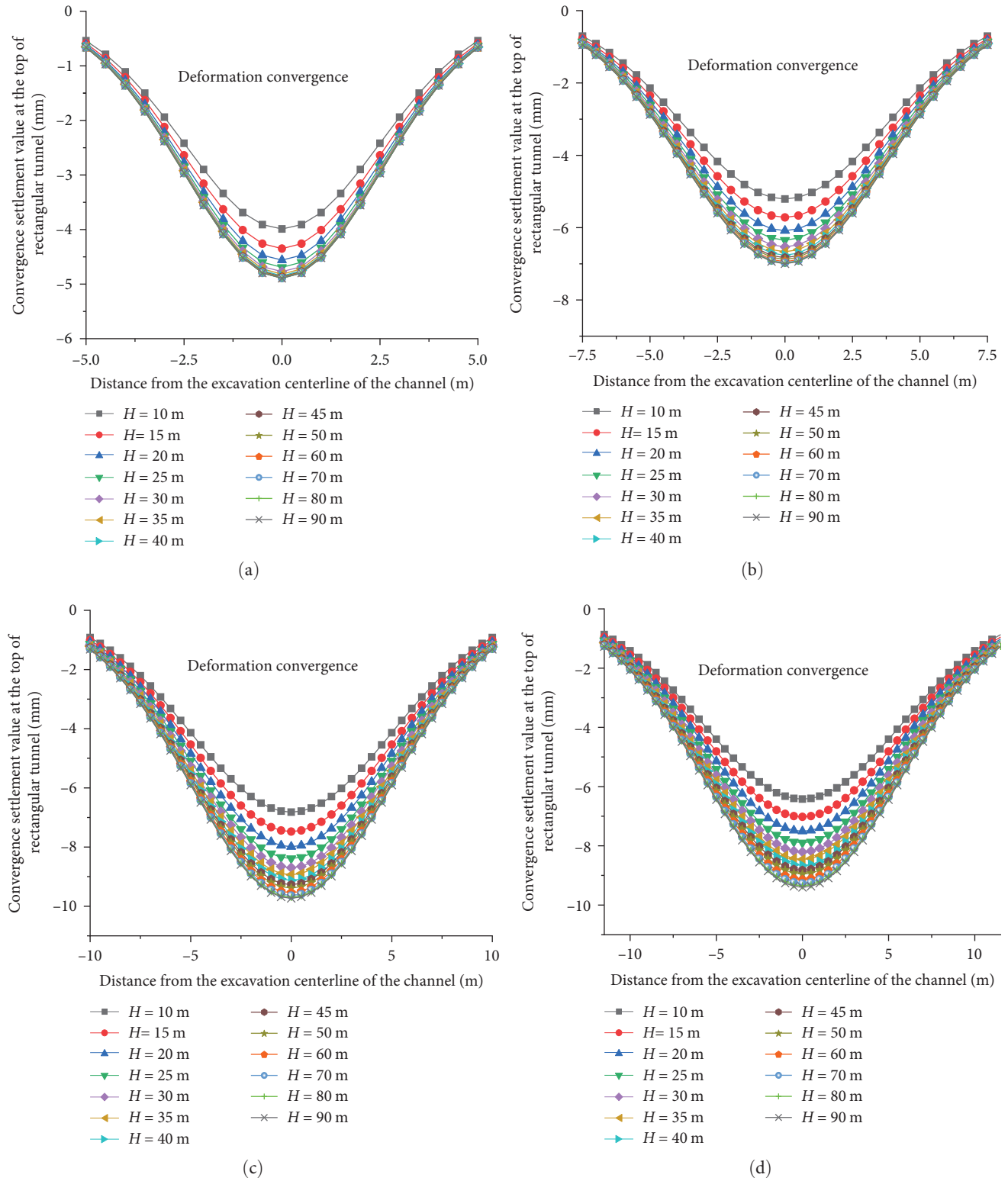

FIGURE 4: Surface convergence of rectangular tunnels with different burial depths: (a) width = 10 m, height = 5 m; (b) width = 15 m, height = 7 m; (c) width = 20 m, height = 10 m; (d) width = 23, height = 9 m.

the following assumptions: (1) the new tunnel and existing tunnel are continuous linear elastic materials (there are no shrinkage cracks); (2) the existing tunnel is in close contact with the surrounding soil; and (3) the geological strata and support structures are considered linear elastic bodies. According to the theory of random media, after obtaining the vertical displacement of the soil, the displacement of the soil at the existing structure is regarded as the displacement

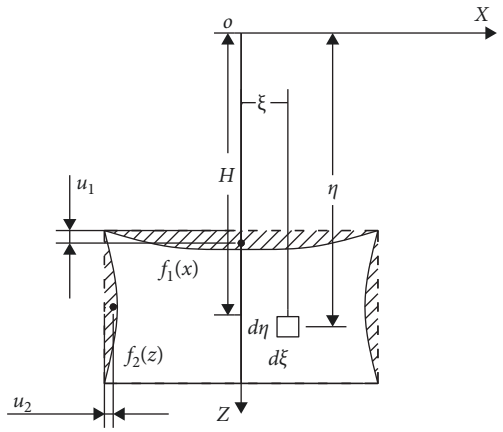

Figure 5: Convergence calculation model of the rectangular tunnel section.

Table 1: Influence of different construction methods on the ground loss rate.

Construction method	V_i (%)
Up and down step method	0.116–1.183
Top heading method	0.333
Central heading method	0.64
Pile underpinning	0.89

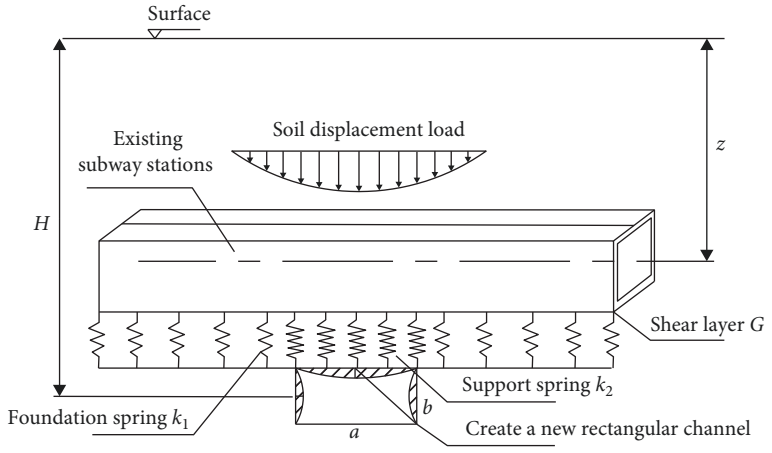

Figure 6: Calculation model of the existing tunnel settlement.

load applied to the existing structure. The simplified analysis is shown in Figure 6, and the vertical displacement of the existing structure is calculated according to the Pasternak foundation model theory.

In Figure 6, $U(x)$ represents the displacement load of the soil, and the vertical displacement of the soil is $u(x)$, while the settlement of the existing tunnel is $w(x)$. According to the assumption of the deformation continuity of the existing tunnel, taking the equivalent foundation coefficient $k = (k_1+k_2)/2$ and using Pasternak foundation model theory, the column balance equation of the beam microsegment can be obtained as follows:

$$EI\frac{d^4w(x)}{dx^4} - GD\frac{d^2w(x)}{dx^2} + kDw(x) = kDu(x). \tag{12}$$

In the equation, EI is the equivalent bending stiffness of the existing structure, G is the shear modulus of the lower strata of the existing structure, and k is the equivalent foundation coefficient. According to the assumption of ground deformation continuity, k can be taken as $k = (k_1 + k_2)/2$, and D is the width of the existing structure.

To obtain the deflection curve of a given structure, we first solve the homogeneous equation by setting the right side

of Equation (12) to $kDu(x) = 0$ and then combining the boundary conditions and the physical meaning of the parameters to obtain the general solution. The general solution is as follows:

It is supposed that $\Delta = (GD)^2 - 4kDEI$; when $\Delta > 0$, the general solution is:

$$w(x) = C_1 e^{\lambda_1 x} + C_2 e^{-\lambda_1 x} + C_3 e^{\lambda_2 x} + C_4 e^{-\lambda_2 x}, \tag{13}$$

where $\lambda_1 = \sqrt{\frac{GD+\sqrt{\Delta}}{2EI}}, \lambda_2 = \sqrt{\frac{GD-\sqrt{\Delta}}{2EI}}$.

When $\Delta = 0$, the general solution is:

$$w(x) = (C_1 + C_2 x)e^{\lambda_1 x} + (C_3 + C_4 x)e^{-\lambda_1 x}, \tag{14}$$

where $\lambda_1 = \sqrt{\frac{GD}{2EI}}$.

When $\Delta < 0$, the general solution is:

$$\begin{aligned} w(x) = {} & (C_1 \cos \lambda_2 x + C_2 \sin \lambda_2 x)e^{\lambda_1 x} \\ & + (C_3 \cos \lambda_2 x + C_4 \sin \lambda_2 x)e^{-\lambda_1 x}, \end{aligned} \tag{15}$$

where $\lambda_1 \pm \lambda_2 \mathrm{i} = \sqrt{\sqrt{\frac{\mathrm{kD}}{4\mathrm{EI}}} + \frac{\mathrm{GD}}{4\mathrm{EI}}} \pm \sqrt{\sqrt{\frac{\mathrm{kD}}{4\mathrm{EI}}} - \frac{\mathrm{GD}}{4\mathrm{EI}}}\mathrm{i}$.

Referring to Zhang and Zhang [20], the boundary conditions and coefficients of the homogeneous equation can be determined by deriving the displacement of a given structure under concentrated loads and nonuniform loads, which will not be elaborated on in this paper. The solution is as follows:

$$w(x,\xi) = \begin{cases} \dfrac{q(\xi)D}{2EI\lambda_1\lambda_2(\lambda_2^2 - \lambda_1^2)}\left(\lambda_2 e^{-\lambda_1|x-\xi|} - \lambda_1 e^{-\lambda_2|x-\xi|}\right), \Delta > 0 \\ \dfrac{q(\xi)D}{4EI\lambda_1^3}(1 + \lambda_1|x-\xi|)e^{-\lambda_1|x-\xi|}, \Delta = 0 \\ \dfrac{q(\xi)D}{4EI\lambda_1\lambda_2(\lambda_2^2 + \lambda_1^2)} e^{-\lambda_1|x-\xi|}(\lambda_2 \cos \lambda_2|x-\xi| + \lambda_1 \sin \lambda_2|x-\xi|), \Delta < 0. \end{cases} \tag{16}$$

The above integral can be solved using MATLAB. Regarding an infinitely long beam, the deflection equation of an elastic beam under any distributed load can be obtained by integrating Equation (16) over $(-\infty, +\infty)$, as follows:

$$w(x) = \int_{-\infty}^{+\infty} w(x,\xi)d\xi. \tag{17}$$

Furthermore, the bending moment and shear force can be obtained by taking the derivative of the deflection curve:

$$M(x) = -EIw''(x), \tag{18}$$

$$Q(x) = -EIw'''(x). \tag{19}$$

3. Engineering Example

To verify the rationality of the above theoretical calculation, based on the construction of the newly built Chengdu Metro Line 27 Jin-Fu Station transfer channel closely crossing the existing Subway Line 6 station, the rationality of the theoretical calculation is verified by comparing it with the numerical simulation results. The specific approach is discussed as follows. (1) Based on the theory of random media, the settlement of the surrounding strata of the existing structure is calculated, the additional load generated by the deformation of the strata is applied to the existing structure, and the settlement of the existing structure is calculated according to the Pasternak foundation beam model theory. (2) A three-dimensional numerical model is established, and finite difference software is used to calculate the deformation of the existing structure. (3) The rationality of the method is verified through the comparison of numerical simulation, theoretical calculation, and measured data.

3.1. Project Overview. The New Jin-Fu Station is a transfer station between Chengdu Metro Line 27 and the existing Line 6, and the new transfer channel closely passes the existing Line 6 station, as shown in Figure 7. The transfer channel is a large-section rectangular tunnel with a flat top and vertical walls: it is 23 m wide, 9 m high, and 25 m deep. Moreover, the bottom plate is approximately 29.17 m from the ground. The existing Line 6 Jin-Fu Station is an island platform station, using a single-column double-span underground two-story cast-in situ frame structure, with a total length of 311.3 m, a standard section width of 20 m, a main station pit depth of approximately 20.26–21.9 m, and a station-covering soil thickness of approximately 5.3 m.

According to the drilling observations, the overlying Quaternary system of the Jin-Fu Station site is entirely artificial fill (Q4 ml); below is a Quaternary system updated upper alluvial layer (Q4al+pl) with clay, powdery clay, clayey powdery soil, medium sand, and gravel. The following soil layers and their parameters are described from top to bottom as follows: mixed fill soil with a layer thickness of 0.53.0 m; plain fill soil with a layer thickness of 0.71.9 m; powdery clay with a layer thickness of 1.12.9 m; clayey powdery soil with a layer thickness of 0.82.4 m; medium sand with a layer thickness of 0.51.3 m; loose gravel with a layer thickness of 1.66.6 m; slightly dense gravel with a layer thickness of

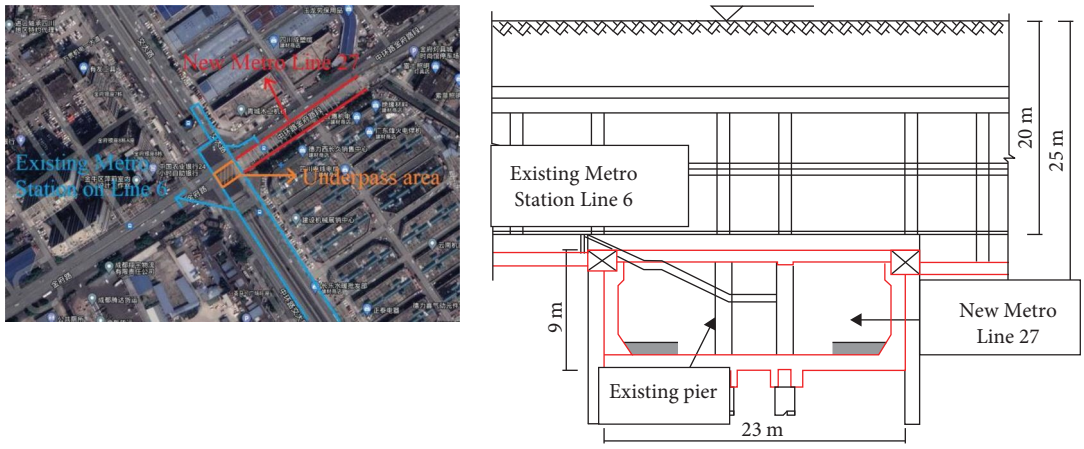

Figure 7: Overhead view and longitudinal section plan; (a) plan view (b) profile digram.

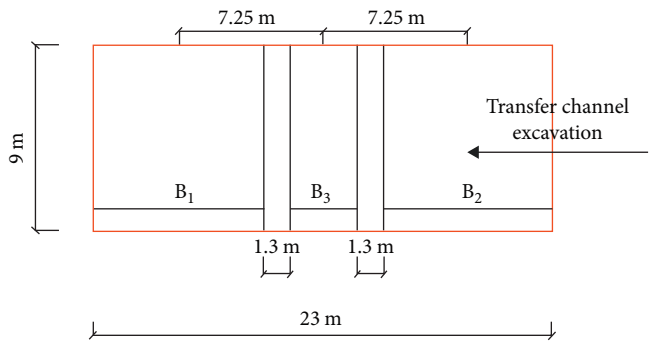

Figure 8: Calculation diagram of the section excavation of the transfer channel.

3.811.9 m; and moderately dense gravel with a layer thickness of 3.116.4 m. The main groundwater at the station is the pore water of the upper stagnant water in the fill layer above the cohesive soil layer and the sand and gravel layer of the Quaternary system, of which the pore water of the sand and gravel layer of the Quaternary system has a greater impact on the engineering, and the hydraulic connection between surface water and groundwater is weak. The groundwater type measured during drilling is mainly pore-type groundwater, and the groundwater level depth is 5.50–7.30 m.

3.2. Existing Station Structure Settlement Theory Calculation

3.2.1. Determination of the Calculation Parameters. The rectangular section size of the interchange channel is $B = 23$ m, $A = 9$ m, and $H = 25$ m. Because there are existing piles extending from the station above in the excavation part of the interchange channel, the excavation section can be divided into three parts, as shown in Figure 8. The existing pile has a diameter of 1.3 m and is considered unexcavated. The widths of the excavation parts are $B_1 = B_2 = 8.5$ m and $B_3 = 3.4$ m, the excavation method adopts the step method, and V_i is taken as 0.46%. The existing station structure section is rectangular and can be regarded as an infinitely long box beam relative to the excavation size. The section height C is 14.86 m, the width D is 20.0 m, the bottom plate burial depth is 20 m, the centerline burial depth is 12.2 m, and the top plate burial depth is 5.14 m. The shear modulus G of the lower strata of the existing station structure can be calculated by the following proposed formula:

$$G = \frac{E_s H_p}{6(1+\nu)}, \tag{20}$$

where E_s is the compression modulus of the lower shear layer soil and Hp is the deformation influence depth of the existing structure, generally taken as 2–4D (that is, 2–4 times the width of the existing structure). According to Equation (20), the shear modulus G of the lower strata of Jin-Fu Station can be calculated as 6.72×10^6 N/m^3.

According to the geological survey report of Jin-Fu Station in Chengdu city, the base coefficient is $k = 3 \times 10^7$ Pa/m, the weighted average of the internal friction angle of each soil layer is 31°, $\tan\beta = 1.05$, the lateral pressure coefficient K is 0.45, and the equivalent stiffness EI is 8.3×10^{13} m^2 based on the concrete strength and section size of the existing structure.

3.2.2. Calculation of the Settlements of Existing Station Structures. Regarding the calculation of u_1 and u_2, according to Equations (8) and (9), when excavating B_1 and B_2, only the convergence u_2 on one side is considered, and the supporting piles do not converge. When excavating B_3, only the upper convergence u_1 is considered, without considering the convergence on both sides. According to Equation (11) and the above parameters, the ground settlement at the centerline burial depth in the existing station structure can be obtained.

$$\begin{aligned} u(x) &= W_1(x-7.4,20)+W_2(x+7.4,20)+W_3(x,20) \\ &= (Bu_{11}+Au_{21})\frac{\tan\beta}{H-20}\exp\left[-\frac{\pi\tan^2\beta}{(H-20)^2}(x-7.4)^2\right] \\ &\quad +(Bu_{12}+Au_{22})\frac{\tan\beta}{H-20}\exp\left[-\frac{\pi\tan^2\beta}{(H-20)^2}(x+7.4)^2\right] \\ &\quad +B_3u_{13}\frac{\tan\beta}{H-20}\exp\left[-\frac{\pi\tan^2\beta}{(H-20)^2}x^2\right]. \end{aligned} \tag{21}$$

According to the above parameters, $\Delta < 0$. Therefore, combined with Equations (16) and (17), the settlement curve of the existing station structure can be obtained.

$$\begin{aligned} w(x) &= \int_{-\infty}^{+\infty} w(x,\xi)d\xi = \int_{-\infty}^{+\infty} \frac{q(\xi)D}{4EI\lambda_1\lambda_2(\lambda_2^2+\lambda_1^2)} \\ &\quad \times e^{-\lambda_1|x-\xi|}(\lambda_2\cos\lambda_2|x-\xi|+\lambda_1\sin\lambda_2|x-\xi|)d\xi. \end{aligned} \tag{22}$$

In this equation, $q(\xi) = ku(\xi)$, $\lambda_1 = 0.0367$ and $\lambda_2 = 0.0366$ according to the above parameters. Similarly, according to Equations (18) and (19), the bending moment and shear force can be calculated.

3.3. Numerical Simulation of the Existing Station Structure. The impact of underpass construction on existing stations is the most significant, as the bottom soil of the station is excavated. Moreover, under the self-weight and upper soil pressure, the existing station is prone to local settlement. During excavation, the existing bottom plate is directly used as the upper structural support, and the existing retaining piles and sidewalls are used as the lateral support structure. Thus, it is easy to disturb the existing station during excavation. To understand the impact of underpass construction on existing stations and reveal the deformation trend of existing structures caused by the construction of rich water sand and pebble formations, it is necessary to simulate the existing station's bottom plate to ensure the safety and normal operation of the existing station.

The simulated area is 240 m in length, 20 m in width and depth, and 60 m in height, and the numerical model established is shown in Figure 9. The calculation process is carried out using large-scale finite difference software. The three-dimensional finite difference calculation model for excavation and construction simulation is divided into 229,574 units and 158,575 nodes. The surrounding rock is assumed to be a continuous medium, and the soil and existing station are simulated using the solid elements, while the structural piles are simulated using pile elements. The plastic deformation of the surrounding rock is considered during excavation using the Mohr—Coulomb constitutive model, while the subway station structure and lining structure are considered to behave only elastically and are thus assigned the linear elastic constitutive model. The calculation parameters are comprehensively determined based on the parameters provided in the geological survey report and engineering experience, and the soil layer parameters are compared with those

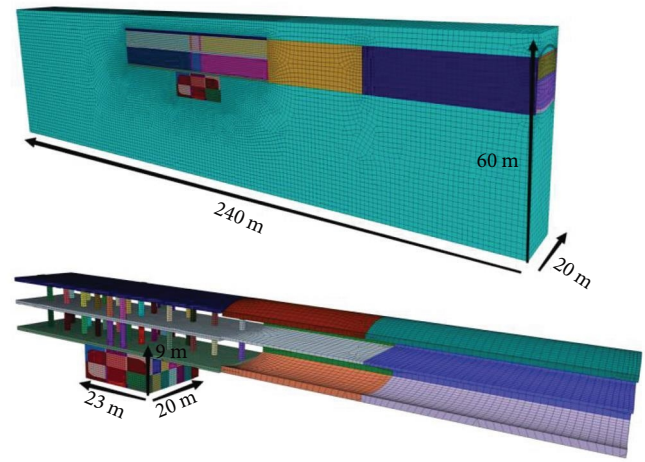

Figure 9: Three-dimensional numerical calculation model.

of the homogeneous soil layers in Table 2. Finally, based on the thickness and the characteristics of the sand and pebble formation, the weighted average value of the soil parameters is used. The station structure is made of C35 reinforced concrete, and the structural piles are made of C30 reinforced concrete. The relevant parameters are taken from the specifications and Table 3.

The surrounding boundary of the calculation model is restrained by roller constraints, the lower surface is restrained by fixed constraints, and the upper surface is restrained by free constraints. The initial stress field considers only the self-weight (including the self-weight of the existing station and the track). According to the actual on-site situation, this section is a busy urban road with a large flow of vehicles and people, so additional loads must be added. During the simulation process, a vertical downward load of 30 kPa is applied to the road surface above the existing station, and in addition, Line 6 is in operation, and the passing train on the track will also produce additional loads. For convenience of study, the train load is assumed to be a static load and is considered uniformly distributed on the track. According to the "Subway Design Code," the general train axle load is 140 kN, which can be regarded as a uniformly distributed load of 40 kN applied on the train track. The model load is shown in Figure 10.

3.3.1. Deformation of the Existing Station Floor. Figure 11 shows the vertical displacement of the existing station floor after the transfer channel is excavated by the numerical simulation. The vertical displacement of the bottom plate near the excavation is the largest, reaching 1.91 mm, followed by the middle layer plate, and the upper layer plate is the smallest. The vertical displacement of the floor is mostly concentrated above the corresponding lower channel, and the farther away it is from the rectangular channel, the flatter the settlement trough of the floor. The range of influence of the settlement trough is within approximately 20 m from the excavation centerline of the rectangular channel. According to Figure 12, after the transfer channel excavation, the

Table 2: Soil layer parameters.

Soil horizon	Thickness (m)	Gravity ($kN \cdot m^{-3}$)	E_s (MPa)	Cohesive strength ($kN \cdot m^{-2}$)	Angle of internal friction (°)	Poisson's ratio (ν)
Miscellaneous fill	1.3	18	11.25	7	10	0.4
Silty clay	2.6	18.5	15.3	20	15	0.35
Loose pebbles	5.6	20	28	0	25	0.32
Slightly dense pebbles	9.1	21	31	0	30	0.31
Medium-dense pebbles	6.8	22	33	0	35	0.3
Dense pebbles	34.6	23	35	0	40	0.29
Weighted average	60	21	33.7	0	31	0.3

Table 3: Material parameters.

Material	Gravity γ ($kN \cdot m^{-3}$)	Elastic modulus E (MPa)	Thickness (m)	Poisson's ratio ν
Columns	27	3.15×10^4	/	0.15
Baseplate	25	3.15×10^4	1.2	0.15
Middle and upper plate	25	3.00×10^4	1.0	0.15
Beam	25	3.15×10^4	/	0.15

Note: The constitutive model of the material shown in Table 3 is elastic, and the cross-sectional area of the beam material is 1.0 m^2, with a moment of inertia of 0.0833 m^4.

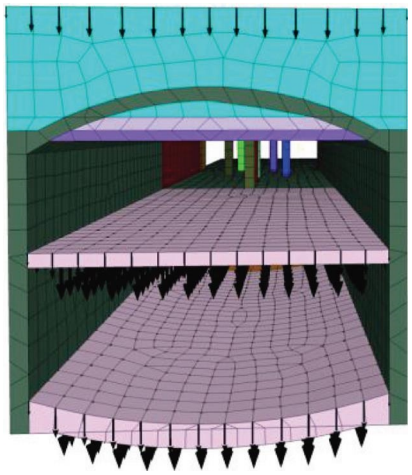

Figure 10: Road and rail load application diagram.

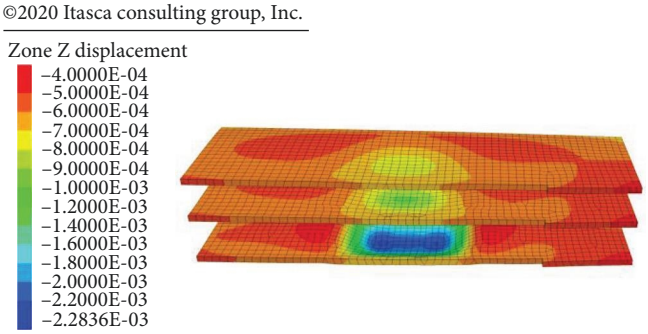

Figure 11: Vertical displacement of the floor after rectangular channel penetration.

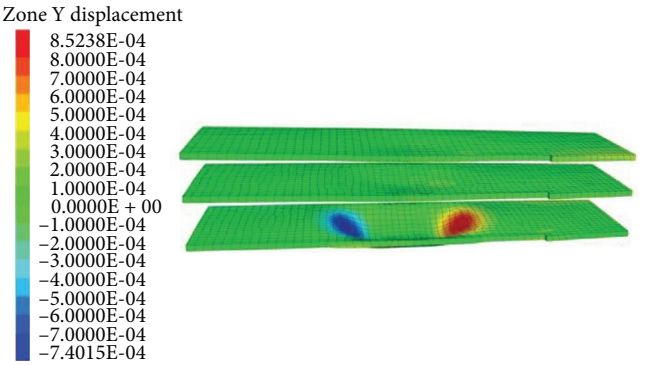

Figure 12: Longitudinal displacement of the floor after rectangular channel penetration.

longitudinal displacement distribution caused by the existing station floor spans across both sides of the bottom plate, and the longitudinal deformation it produces approaches the excavation centerline. The maximum longitudinal displacement of the bottom plate is 0.85 mm, while the longitudinal displacement of the middle and upper layers is negligible. The farther it is from the transfer channel, the smaller the lateral displacement of the floor. The magnitude of the longitudinal displacement is related to the depth of the settlement groove. The maximum lateral displacement is produced by the maximum settlement magnitude of the bottom plate. This is because while the settlement groove is formed, the bottom plate undergoes bending deformation, and the two sides of the settlement center are subjected to the tensile stress. The greater the depth of the settlement groove, the greater the tensile stress it receives.

3.3.2. Existing Station Column Deformations. After the excavation of the transfer channel, the force and deformation of

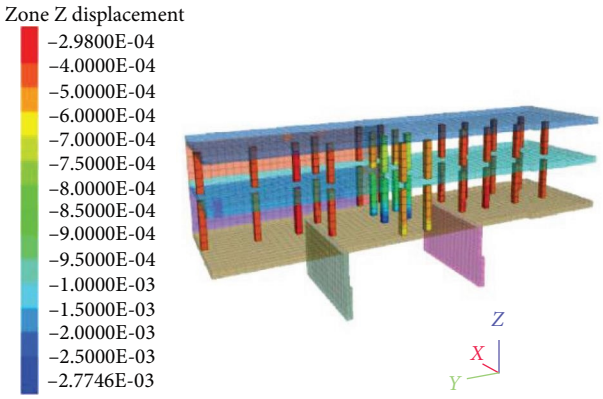

Figure 13: Vertical displacement of the column after the channel passes underneath.

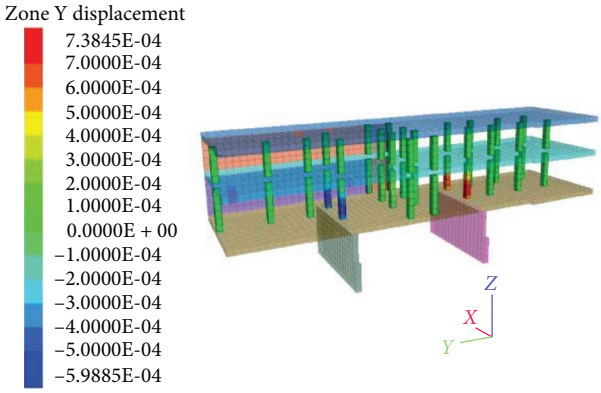

Figure 14: Longitudinal displacement of the column after the channel passes underneath.

the existing station columns changed. Figures 13 and 14 are the vertical and longitudinal displacement contour maps of the columns after the channel was excavated. These figures show that the maximum vertical displacement is 2.3 mm, mainly occurring at the columns near the top of the transfer channel; the maximum longitudinal displacement is 0.74 mm, mainly occurring at the columns above the end walls of the transfer channel. The sizes of the displacement values indicate that the excavation of the transfer channel has the greatest impact on the vertical displacement of the columns, followed by the impact on the longitudinal displacement. The displacement of the bottom columns is greater than that of the upper columns of the station. With the excavation of the transfer channel, there are two aspects that affect the columns. One aspect is that the excavation of the bottom soil of the existing station leads to a decrease in the support force at the bottom of the columns, resulting in vertical displacement. The second is that the longitudinal deformation of the bottom plate drives the columns to produce longitudinal deformation, leading to an increase in the shear force of the columns above the sidewalls. The maximum shear force diagram of the existing station columns in Figure 15 shows that the shear force of the existing station columns is mainly concentrated on both sides from the transfer channel, and the shear force of the columns directly above the channel is relatively small.

3.3.3. Overall Deformation and Force of the Existing Station. Analyzing the deformation and force of the overall structure of the existing station and exploring the impact of underpass construction on the existing station can reveal the deformation and force trends of the existing station. Figure 16 shows that the overall structure of the station sinks and that the structural deformation mainly occurs in the bottom plate and columns above the channel. The settlement magnitude increases closer to the excavation channel. As the distance between the existing station and the excavation channel increases, the settlement magnitude gradually decreases. At the same time, the existing sidewalls on both sides of the excavation channel deform toward the inside of the channel, with smaller deformations at the upper and lower ends and larger deformations at the middle. According to the maximum shear force diagram of the overall structure of the station in Figure 17, the shear stress of the columns above the sidewalls of the channel toward the outside of the channel is larger than that of the columns toward the inside. The maximum shear stress appears at the columns directly above the sidewalls of the channel. In addition, compared with the middle and upper plates, the bottom plate produces a larger shear force. Considered comprehensively, the bottom plate and columns above the sidewalls of the channel are the most unfavorable shear planes, which is consistent with the theoretical calculation results.

3.4. Results Analysis and Comparison. Figure 18 shows the theoretical calculation, numerical simulation, and measured results of the deformation of the existing station's base plate. The impact range of the existing station is basically between −100 and 100 m, which is approximately 5 times the excavation width. The maximum settlement magnitudes of the existing station's base plate under the measured data, numerical simulation, the calculation in this paper, and the traditional random medium theory are 1.91, 1.95, 2.11, and 2.76 mm, respectively. The traditional random medium theory calculation values are larger than the actual values, with an error of 0.85 mm, while the theoretical calculation part in this paper (as shown in Section 2) is based on the improved stochastic media theory and analyzed using the two-stage method. Despite making a series of assumptions, such as neglecting the interaction between soil and structure, the comparison of the improved theoretical calculation results with numerical simulations and field measurements revealed that the sizes and patterns of the three datasets are basically consistent. Through analysis, it is found that the theoretical calculation values are slightly larger than the measured values because there are piles extending from the base plate of the station above as supports along the centerline of the new tunnel in the actual conditions, which have some constraints on the settlement of the base plate. To reflect the deformation of the existing structure more realistically, pile structure elements were added to support the existing station in the numerical simulation part. The simulation values are basically consistent with the measured data. In contrast, the constraint of the existing station by the retaining piles is not fully considered in the theoretical calculation. Only the

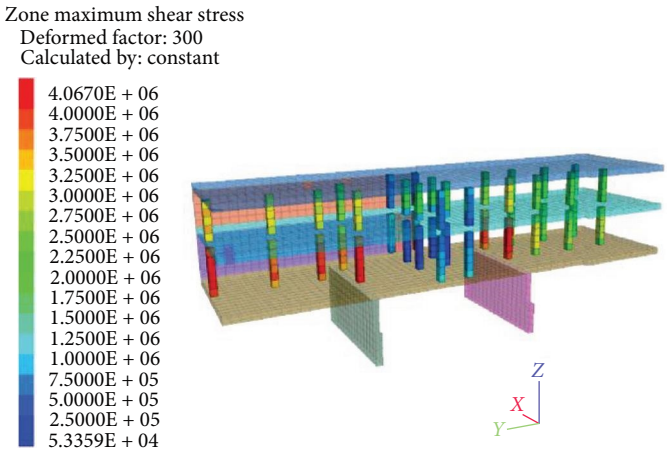

Figure 15: Maximum shear force of the column after the channel passes underneath.

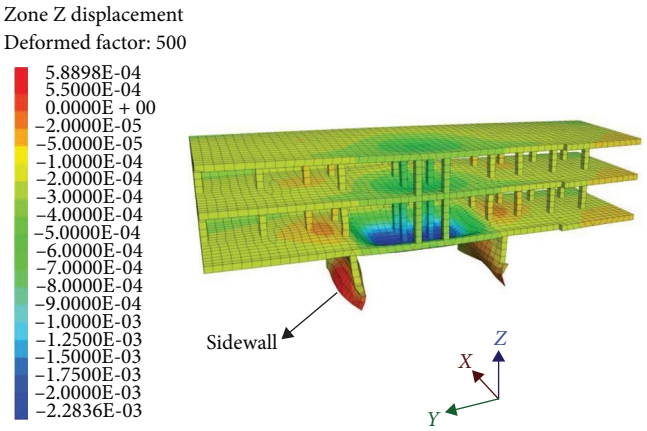

Figure 16: The whole structure of the station is deformed after underpass construction.

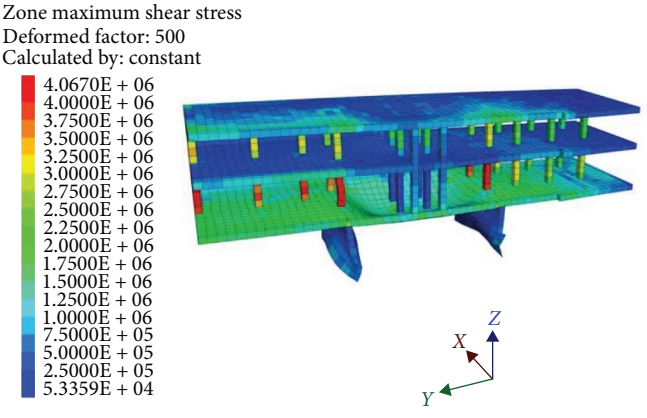

Figure 17: Maximum shear force of the station structure after underpass construction.

retaining piles were calculated as nonexcavated partition walls. As a result, there were differences in the settlement magnitudes, but overall, the theoretical calculation results reflected the settlement characteristics of the existing station structure to some extent.

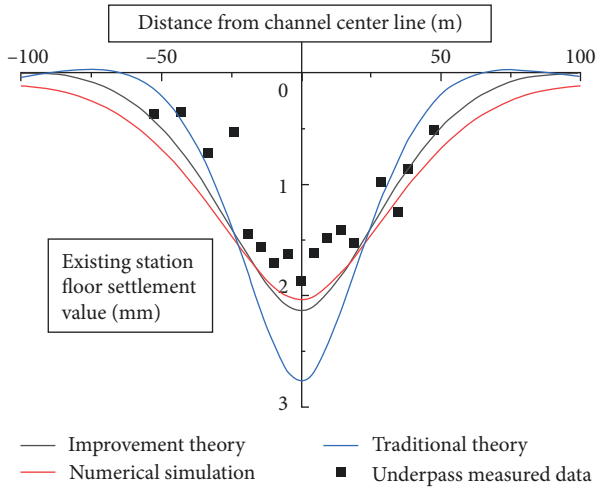

Figure 18: Subsidence curve of the existing station floor.

As shown in Figures 19 and 20, the longitudinal bending moment curve of the existing station floor is convex in the middle and concave on both sides. On both sides, 7.25 and 45 m from the centerline of the transfer channel, the existing station floor bears the maximum positive bending moment and the maximum negative bending moment, respectively. The maximum positive bending moment of the existing station floor is not at the centerline of the excavation surface because the existence of the existing station's bottom support piles changes the stress characteristics of the floor, causing the maximum bending moment of the floor to shift from the centerline to both sides and causing a "concave groove" phenomenon. In addition, the maximum longitudinal shear force of the existing station floor occurs at $x = \pm 11.5$ m, where the floor structure will bear the maximum shear force. The existing station is prone to failure such as overturning and shearing in this area, so protective measures should be included for the above three most unfavorable positions in design and construction. In summary, the use of the combination of the improved random medium theory and the Pasternak foundation model to analyze the mechanical response of the

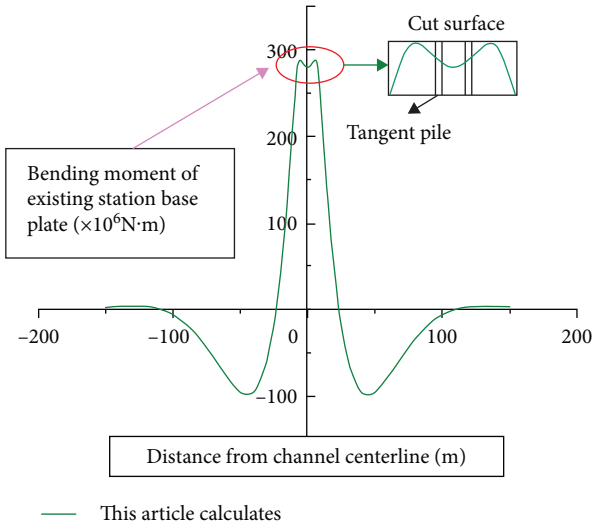

Figure 19: Longitudinal moment of the existing station floor.

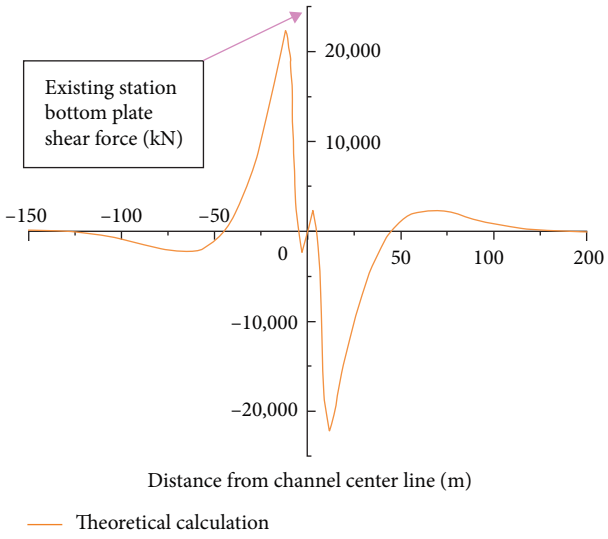

Figure 20: Longitudinal shear of the existing station floor.

existing station is feasible, and further research can be conducted on the longitudinal response characteristics of the existing station.

4. Parametric Sensitivity Analysis

The value of the net distance determines the size of the displacement load applied to the existing station, and the width-to-height ratio of the excavation section is also an important factor affecting deformation. In addition, the foundation reaction coefficient is a key parameter that reflects the interaction between the existing station and the soil. Therefore, to study the mechanical response of the existing station to the construction of undercrossing, the net distance d, the height-to-width ratio A/B, and the foundation reaction coefficient k, which are parameters of the undercrossing of the existing

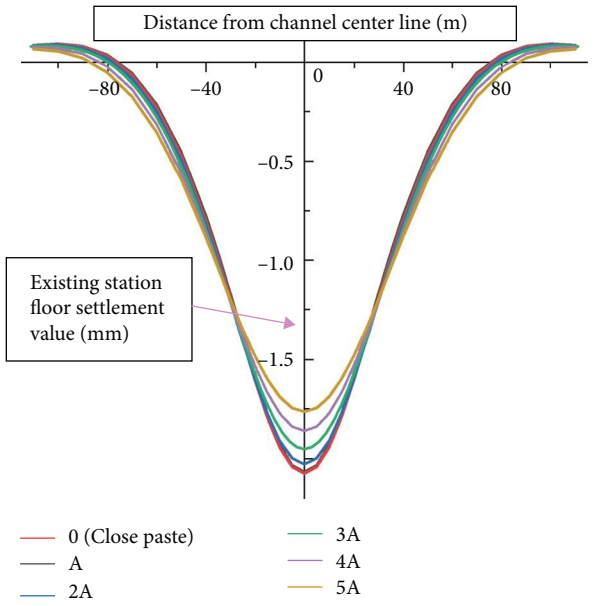

Figure 21: Subsidence curve of the existing station floor under different net distances.

station at Jin-Fu Station on Line 27 in Chengdu, are used as the standard to analyze the three influencing factors.

4.1. The Net Distance between the Transfer Channel and the Existing Station Is d. The stress and strain of the existing station are closely related to the net distance d. When a new channel is excavated under construction, with the increase in the net distance, a certain height of the arch structure will be formed on the top of the intermediate layer soil, and the height of the tunnel collapse arch is related to the thickness of the intermediate layer soil. Therefore, it is necessary to study the net distance d between the transfer channel and the existing station. Under the condition that the soil parameters, the excavation size of the channel, and the burial depth of the existing structure remain unchanged, the net distance d is studied by considering net distances of 0 (tight contact), A, $2A$, $3A$, $4A$, and $5A$, where A is the height of the transfer channel, and other physical parameters remain unchanged during calculation.

Figure 21 shows that the settlement of the bottom plate of the existing structure decreases with increasing net distance, and the settlement magnitude of the bottom plate of the existing structure is the largest when the net distance is 0 (tight contact). When the net distance does not exceed $2A$, the maximum settlement magnitude of the existing station decreases relatively slowly. When the net distance exceeds $2A$, the settlement magnitude of the existing station begins to decrease rapidly. Afterward, as the net distance further increases, the distance between the new tunnel and the existing structure above it continues to increase, its influence on the existing structure decreases, and the trend of settlement magnitude change uniformly reduces. Comparing the settlement change curve of the existing structure under different intermediate layer soils, it can be seen that when the net distance d is small, due to the small thickness of the

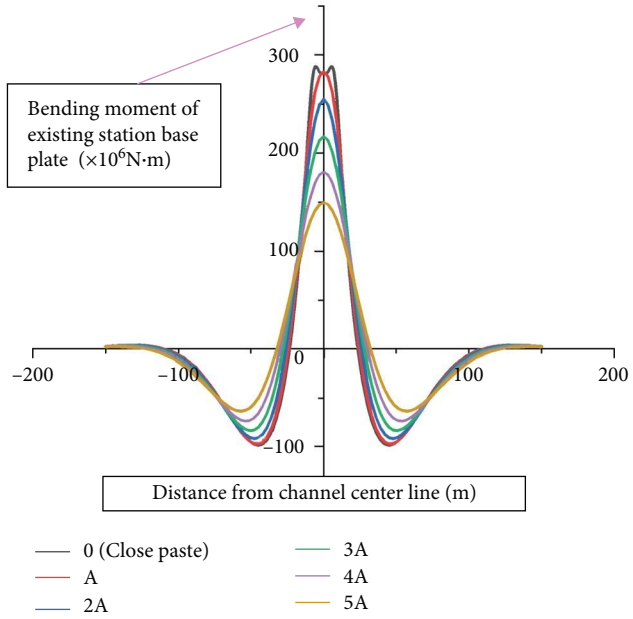

Figure 22: Longitudinal bending moment of the existing station floor under different net distances.

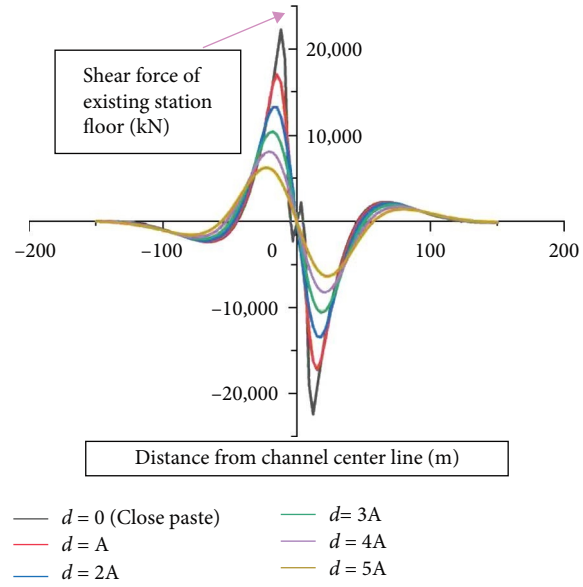

Figure 23: Longitudinal shear force of existing station floor under different net distances.

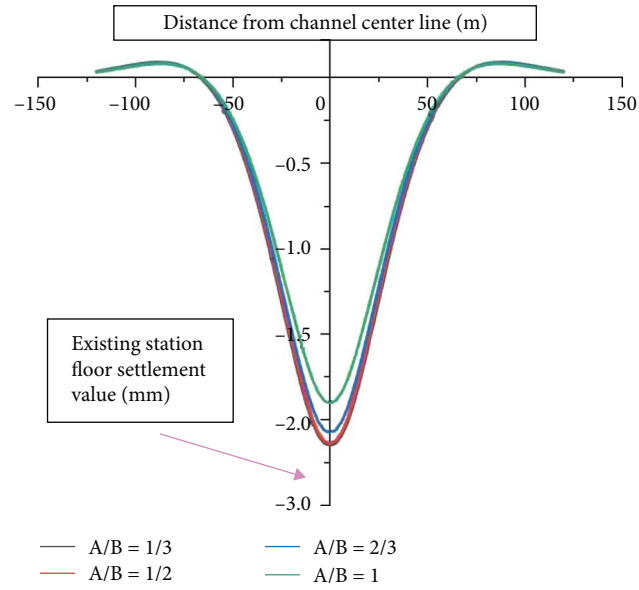

Figure 24: Settlement curve of the existing station floor under different height-to-width ratios.

intermediate layer soil, the soil arch structure cannot be effectively formed. At the same time, due to the increase in the burial depth, the self-weight of the soil above the transfer channel increases, resulting in an increase in the convergent area of the excavation surface of the transfer channel and an increase in the stratum loss rate. Therefore, the deformation of the existing station is basically not much different from that expected with tight contact. When the net distance d is large, the thickness of the intermediate layer soil of the transfer channel and the existing station increases, forming a soil arch structure. Since the formation of the arch structure of the interlayer soil can increase the stability of the upper existing station, the settlement magnitude of the existing station decreases rapidly at this time.

Figures 22 and 23 show that both the bending moment and shear force of the existing station decrease with increasing net distance. As the net distance increases from 0 to 5A, the maximum bending moment and shear force decrease by 46.4% and 72.9%, respectively. It can also be found that the bending moment "notch" phenomenon only occurs when the tunnel is in tight contact. After the net distance increases, interlayer soil is generated between the transfer channel and the existing station, and the bending moment "notch" phenomenon disappears. Therefore, a certain thickness of interlayer soil can reduce the mechanical response of the existing station. Thus, it is possible to reserve a certain net distance in the design of the underpass of the existing station while meeting the usage requirements.

4.2. The Height-to-Width Ratio of the Excavation Surface. The height-to-width ratio A/B of the excavation surface is an important parameter for the displacement of soil layers in random media theory. The displacement load generated by this ratio is different from the mechanical response of the existing station. Therefore, under the conditions of maintaining the tight fit, constant excavation area, and constant support pile position, different height-to-width ratios A/B of 1/3, 1/2, 2/3, and 1 were selected for analysis and comparison. Here, A and B represent the height and width of the excavation surface, respectively.

As shown in Figure 24, as the height-to-width ratio of the excavation cross-section increases from 1/3 to 1, the magnitude of settlement of the existing station's bottom plate decreases from 2.15 to 1.90 mm, and the settlement gradually decreases as the height-to-width ratio increases. When the height-to-width ratio increases from 1/3 to 1/2, the magnitude of settlement decreases from 2.15 to 2.13 mm, and the

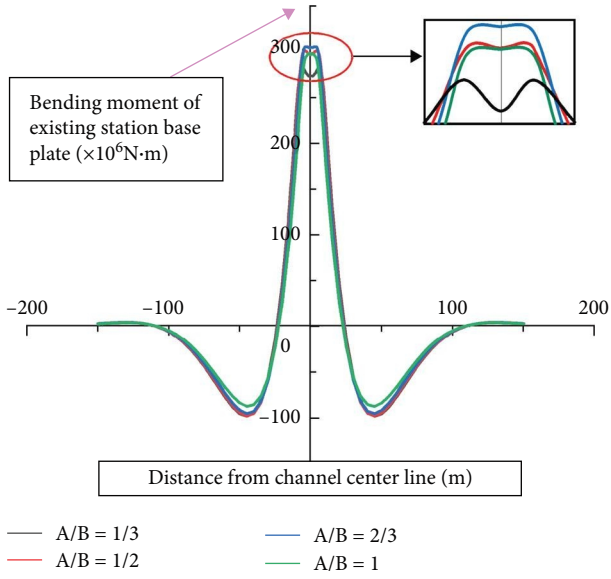

Figure 25: Longitudinal bending moment of the existing station floor under different height-to-width ratios.

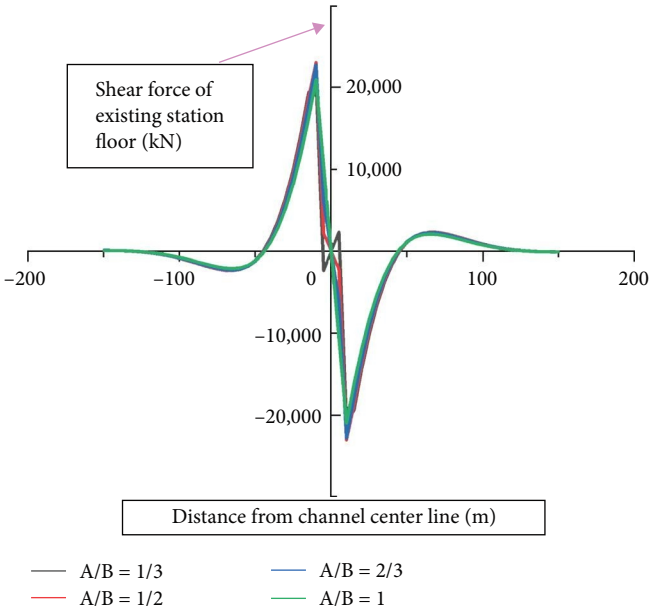

Figure 26: Longitudinal shear force of the existing station floor under different height-to-width ratios.

change is not significant. However, when it increases from 1/2 to 1, the magnitude of settlement decreases more significantly. The magnitude of settlement decreases from 2.13 to 1.90 mm, which is a reduction of 10.8%. This is because under the condition of a constant excavation area, the increase in the height-to-width ratio indirectly leads to a decrease in the span of the excavation cross-section, which in turn reduces the convergence area of the cross-section and the displacement load acting on the existing station. In addition, because the transfer channel is closely penetrated, the reduction in span can effectively reduce the exposed area of the existing station's bottom plate. When the exposed area is less than a certain value, it can effectively reduce the magnitude of settlement of the existing station.

Through the analysis of Figures 25 and 26, it can be seen that as the height-to-width ratio increases from 1/3 to 2/3, the maximum positive bending moment of the existing station floor gradually increases, and the maximum negative bending moment gradually decreases. However, when the height-to-width ratio increases from 2/3 to 1, the maximum positive bending moment of the existing station floor begins to decrease, and the maximum negative bending moment continues to decrease; with the change in the height-to-width ratio, the shear force remains basically unchanged. When the height-to-width ratio increases to 2/3, the "concave groove" of the bending moment begins to decrease. This is because as the height-to-width ratio increases, spans B_1 and B_2 outside the supporting piles decrease, and the point of maximum positive bending moment begins to shift toward the center point. Therefore, considering the deformation and stress of the existing station, a height-to-width ratio between 2/3 and 1 can be selected according to the actual situation, and large-span excavation sections should be avoided as much as possible.

4.3. Coefficient of Subgrade Reaction k. To study the longitudinal mechanical response of the existing station under different foundation reaction coefficients and reasonably select the foundation reaction coefficient, based on the foundation coefficient $k = 3 \times 10^7$ Pa/m in 2.2.1, four different foundation reaction coefficients of $0.1k$, $0.5k$, $1.0k$, and $10k$ were used to conduct research on the above analytical solution under the condition that the above condition parameters are unchanged.

Through analysis of Figure 27, it can be seen that as the foundation reaction coefficient increases, the interaction between the station floor and the foundation gradually increases, resulting in a gradual reduction in the displacement influence range of the station floor, but the maximum settlement magnitude gradually increases, reaching a maximum of 3.4 mm, and the shape of the settlement curve of the floor changes from "shallow and wide" to "deep and narrow". For example, when the coefficient is $0.1k$, the displacement influence range is −100–100 m, and the maximum settlement magnitude is 1.25 mm. When the coefficient increases to $10k$, the displacement influence range is −75–75 m, and the maximum settlement magnitude is 3.4 mm, which is an increase of 2.72 times. In addition, Figures 28 and 29 show that as the foundation reaction coefficient increases from $0.1k$ to $10k$, the bending moment and shear force values increase rapidly, increasing by 14.9 times and 51.7 times, respectively, compared with before, which indicates that the influence of the foundation reaction coefficient on the force of the existing station is significant. Taking $1.0k$ as an example, the longitudinal bending moment of the floor is distributed in the form of a central protrusion and two concavities, and the maximum positive and negative bending moments are located on both sides of the centerline of the transfer channel at 7.25 and 45 m, respectively. The floor is in the most unfavorable tensile and

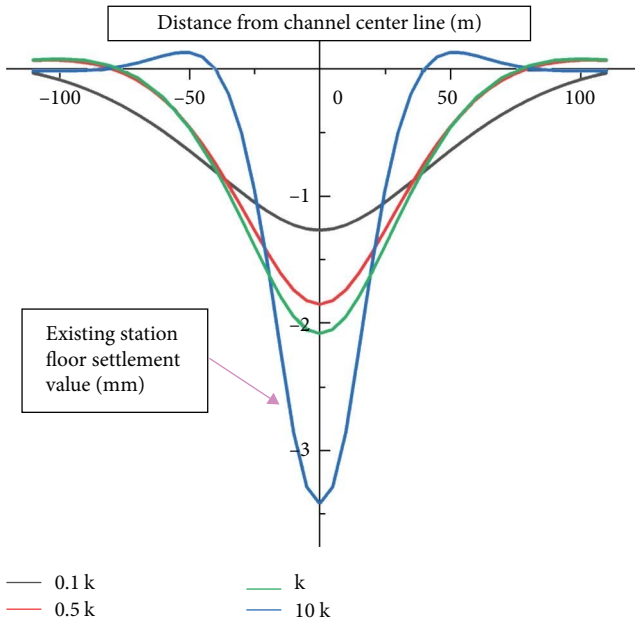

Figure 27: Subsidence curve of the existing station floor under different foundation counterforce coefficients.

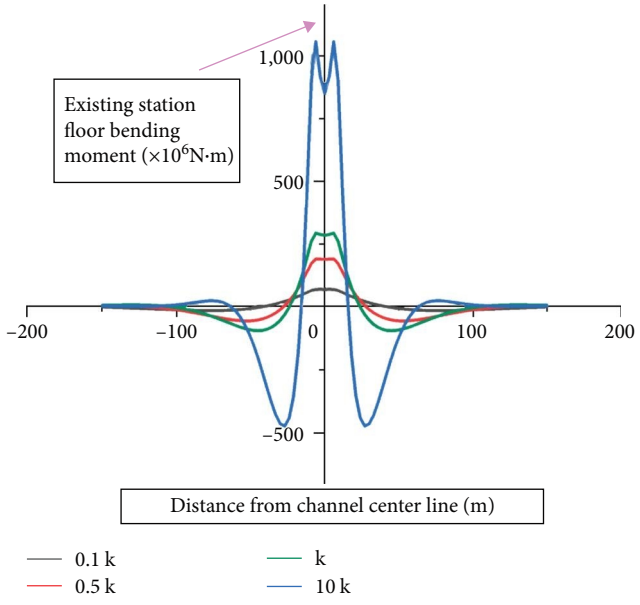

Figure 28: Longitudinal moment of the existing station floor under different foundation counterforce coefficients.

compressive state; the longitudinal shear force of the floor is distributed in an inverted Z-shape, and the maximum shear force appears on both sides of the centerline at 11.5 m, where the floor is susceptible to shear failure due to step cutting. In summary, the reasonable selection of the foundation reaction coefficient is the key to accurately calculating the mechanical response of the existing station. To ensure the safe operation of the existing station, the foundation reaction coefficient can be appropriately increased to ensure the safety of the construction of the underpass.

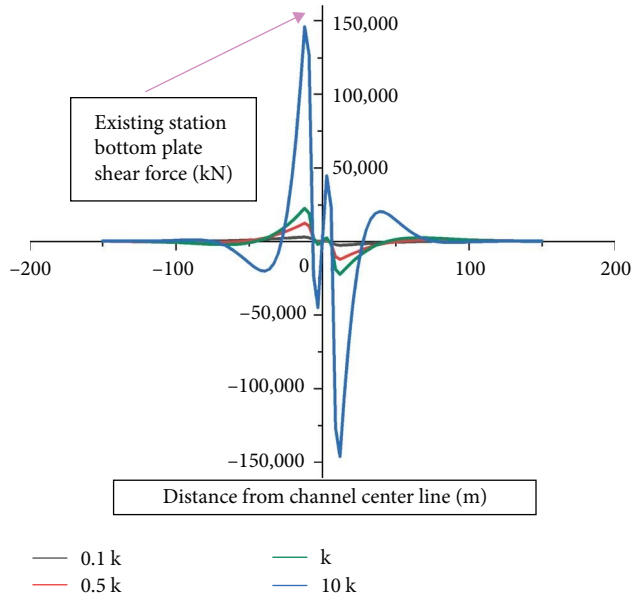

Figure 29: Longitudinal shear force of the existing station floor under different foundation reaction coefficients.

5. Conclusion

(1) After excavation, the rectangular tunnel section will produce uneven convergence, and its boundary is a nonlinear curve rather than a straight line. In this regard, the integration boundary of the section in the traditional random medium theory was improved to make theoretical calculations more biased toward the actual conditions. In addition, the traditional random medium theory was simplified to make the calculation more convenient. Through a comparison of results, it was found that the calculation in this paper is more in line with the actual measured data, which verifies the feasibility of the theory in this paper.

(2) The influence range of the settlement of the existing station's base plate is between −100 and 100 m. The longitudinal bending moment curve is convex in the middle and concave at the two sides. The maximum positive bending moment and the maximum negative bending moment occur on both sides 7.25 and 45 m from the centerline of the transfer channel, respectively. At the same time, the constraint of the support piles causes the base plate at the center of the excavation to exhibit a bending moment "trough" phenomenon. In addition, the most unfavorable shear surface appears on both sides 11.5 m from the centerline.

(3) With the increase in the net distance d parameter, the most unfavorable part of the base plate will shift outside the centerline. Maintaining a certain net distance d (that is, increasing the interlayer soil thickness) is conducive to the formation of the soil arch effect, reducing the deformation of the upper existing station and the bending moment and shear force of the existing station's base plate. With the increase in the height-to-width ratio A/B, the settlement

magnitude of the existing station's base plate decreases, but it also increases the maximum bending moment of the base plate to a certain extent. When the height-to-width ratio reaches 1, the maximum bending moment begins to decrease, but at this time, the change in the bending moment compared with the original bending moment of the existing station's base plate can be ignored. With the increase in the foundation reaction coefficient k, the interaction between the soil and the existing station is enhanced, and the deformation, bending moment, and shear force of the existing station's base plate increase significantly. When the foundation reaction coefficient increases to $10k$, a more obvious uplift phenomenon occurs outside the settlement groove of the existing station's base plate.

Data Availability

Data supporting in this research article are available on request.

Conflicts of Interest

The authors declare that they have no known competing financial interests or personal relationships that could have appeared to influence the work reported in this paper.

Authors' Contributions

Houqiang Sun and Yu Du contributed in the validation. Yu Du, Houqiang Sun, and Lirong Teng contributed in the supervision. Jun Wu and Houtong Qin contributed in the methodology. Jun Wu contributed in the investigation. Jiabing Zhang and Houtong Qin contributed in software. Jiabing Zhang contributed in the funding acquisition.

Acknowledgments

This study was financially supported by the National Natural Science Foundation of China (Grant No. 52108367) and the Science and Technology Department of Guangxi Zhuang Autonomous (Grant No. AD21238018). The authors also express special thanks to the editors and anonymous reviewers for their constructive comments.

References

[1] R. Liang, T. Xia, Y. Hong, and F. Yu, "Effects of above-crossing tunnelling on the existing shield tunnels," *Tunnelling and Underground Space Technology*, vol. 58, pp. 159–176, 2016.

[2] X. Weng, H. Yu, H. Niu, J. Hu, W. Han, and X. Huang, "Interactive effects of crossing tunnel construction on existing tunnel: three-dimensional centrifugal test and numerical analyses," *Transportation Geotechnics*, vol. 35, Article ID 100789, 2022.

[3] Y. B. Liu, S. M. Liao, L. S. Chen, and M. B. Liu, "Structural responses of DOT tunnel induced by shield under-crossing in close proximity in soft ground. part I: field measurement," *Tunnelling and Underground Space Technology*, vol. 128, Article ID 104623, 2022.

[4] J. Han, J. Wang, C. Cheng et al., "Mechanical response and parametric analysis of a deep excavation structure overlying an existing subway station: a case study of the Beijing subway station expansion," *Frontiers in Earth Science*, vol. 10, Article ID 1079837, 2023.

[5] R.-P. Chen, X.-T. Lin, X. Kang et al., "Deformation and stress characteristics of existing twin tunnels induced by close-distance EPBS under-crossing," *Tunnelling and Underground Space Technology*, vol. 82, pp. 468–481, 2018.

[6] Z. Zhou, Y. Chen, and L. Miao, "Study of equivalent layered method based prediction model for deformations caused by construction of new tunnels undercrossing existing tunnels," *Modern Tunnelling Technology*, vol. 57, no. 5, pp. 99–103, 2020.

[7] X. Liu, Q. Fang, D. Zhang, and Z. Wang, "Behaviour of existing tunnel due to new tunnel construction below," *Computers and Geotechnics*, vol. 110, pp. 71–81, 2019.

[8] C. Zhao, M. Lei, C. Shi, H. Cao, W. Yang, and E. Deng, "Function mechanism and analytical method of a double layer pre-support system for tunnel underneath passing a large-scale underground pipe gallery in water-rich sandy strata: a case study," *Tunnelling and Underground Space Technology*, vol. 115, Article ID 104041, 2021.

[9] X. Liu, A. Jiang, Q. Fang, Y. Wan, J. Li, and X. Guo, "Spatiotemporal deformation of existing pipeline due to new shield tunnelling parallel beneath considering construction process," *Applied Sciences*, vol. 12, no. 1, Article ID 500, 2022.

[10] G. Wei, G. H. Yu, and B. Yang, "Calculation of existing shield tunnel shearing dislocation platform deformation due to undercrossing new shield tunnel undercrossing," *Journal of Hunan University Natural Sciences*, vol. 45, no. 9, pp. 103–112, 2018.

[11] X. Y. Wang, K. Lei, and T. Wang, "Prediction of existing pipeline settlement resulting from the construction of an underground metro station using the pile–beam–arch (PBA) method," *China Civil Engineering Journal*, vol. 54, no. S1, pp. 65–75, 2021.

[12] W. H. Ke, L. X. Guan, and D. H. Liu, "Research on upper pipeline-soil interaction induced by shicld tunnellin," *Rock and Soil Mechanics*, vol. 41, no. 1, pp. 221–228, 2020.

[13] H. Lai, H. Zheng, R. Chen, Z. Kang, and Y. Liu, "Settlement behaviors of existing tunnel caused by obliquely under-crossing shield tunneling in close proximity with small intersection angle," *Tunnelling and Underground Space Technology*, vol. 97, Article ID 103258, 2020.

[14] J. Litwiniszyn, "Application of the equation of stochastic processes to mechanics of loose bodies," *Archiwum Mechaniki Stosowanej*, vol. 8, pp. 393–411, 1956.

[15] X. Han and N. Li, "Comparative analysis of strata prediction models for ground movement induced by tunnel construction," *Chinese Journal of Rock Mechanics and Engineering*, vol. 26, no. 3, pp. 594–600, 2007.

[16] H. A. N. Xuan and L. I. Ning, "A predicting model for ground movement induced by non-uniform convergence of tunnel," *Chinese Journal of Geotechnical Engineering*, vol. 29, no. 3, pp. 347–352, 2007.

[17] A. Verruijt and J. R. Booker, "Surface settlements due to deformation of a tunnel in an elastic half plane," *Géotechnique*, vol. 46, no. 4, pp. 753–756, 1996.

[18] J. Wang, D. L. Zhang, C. P. Zhang, Q. Fang, J. Su, and N. Du, "Deformation characteristics of existing tunnels induced by excavation of new shallow tunnel in Beijing," *Chinese Journal of Rock Mechanics and Engineering*, vol. 33, no. 5, pp. 947–956, 2014.

[19] X. U. Qiang, Z. H. U. Yongquan, L. E. I. Shengxiang et al., "An improved stochastic medium theoretical model for predicting the deformation ofexisting tunnels and strata caused by the excavation of new tunnels undercrossing existing tunnels," *Chinese Journal of Geotechnical Engineering*, vol. 45, no. 2, pp. 301–309, 2023.

[20] H. Zhang and Z. X. Zhang, "Vertical deflection of existing pipeline due to shield tunnelling," *Journal of Tongji University (Natural Science)*, vol. 41, no. 8, pp. 1172–1179, 2013.